Topological Phase Diagram of $Pb_{1-x}Sn_xSe_{1-y}Te_y$ Quaternary Compound

G. Cuono[a,*], G. Hussain[a],
A. Fakhredine[b] and C. Autieri[a]

[a] *International Research Centre MagTop, Institute of Physics, Polish Academy of Sciences, al. Lotników 32/46, PL-02668 Warsaw, Poland*
[b] *Institute of Physics, Polish Academy of Sciences, al. Lotników 32/46, PL-02668 Warsaw, Poland*

Received: 30.06.2022 & Accepted: 23.09.2022

Doi: 10.12693/APhysPolA.142.521 *e-mail: gcuono@magtop.ifpan.edu.pl

We reproduce the mirror Chern number phase diagram for the quaternary compound $Pb_{1-x}Sn_xSe_{1-y}Te_y$ combining the accurate density functional theory and the tight-biding model. The tight-binding models are extracted from the *ab initio* results, adding constraints to reproduce the experimental results. By using the virtual crystalline approximation, we calculated the mirror Chern number as a function of the concentrations x and y. We report different Hamiltonians depending on whether we want to focus on the experimental band gap or the experimental topological transition. We calculate the transition line between the trivial insulating phase and the topological insulating phase, which agrees well with the experimental results. Finally, we add the predicted in the literature Weyl phase into the phase diagram, providing a complete topological phase diagram for the $Pb_{1-x}Sn_xSe_{1-y}Te_y$ quaternary compound.

topics: topological crystalline insulator, mirror Chern number, Weyl phase, alloys

1. Introduction

In the last decade, there has been a new interest in the investigation of narrow gap semiconductors and semimetals due to the chance of magnetism engineering [1–5], topological insulator phases [6, 7], Dirac and Weyl phases [8–11], quantum spin Hall phases [12], nodal-line phases [13, 14], axion insulating phase [15, 16], and flat bands [17]. Indeed, heterostructures and doping allow to manipulate the electronic, optical, and magnetic properties producing new phases [18–24]. Among these phases, topological crystalline insulators (TCI) are a state of matter in which the topological nature of the electronic structure arises from the crystal lattice [25]. Surface bands of TCI are low-energy states occurring along certain high-symmetry directions [26–28]. Topological surface states in TCI are protected by crystalline space group symmetries, but not the time-reversal symmetry (as in the case of the conventional Z_2 topological insulators (TI) [29]). Topological crystalline phase has also been found in semimetallic systems [30, 31], while topological crystalline metallic phases have been deeply investigated mainly in orthorhombic crystal structure [32–40] as well as in other transition metal pnictides with quasi-one-dimensional structure [41–44], where the coexistence of topology and superconductivity has been predicted.

IV–VI semiconductors [45] exhibit many properties such as thermoelectricity [46, 47], ferroelectricity [48, 49], superconductivity [50, 51], and zero-energy modes [52, 53]. These compounds are used for applications in spintronics [54, 55] and optoelectronics [56, 57]. Much of the interest in these materials stems from the recent discovery of the topological crystalline insulating phase in SnTe [25, 58, 59] and some of their substitutional alloys [60–62] such as $Pb_{1-x}Sn_xTe$ [60], $Pb_{1-x}Sn_xSe$ [61], and $Pb_{1-x-y}Sn_xMn_yTe$ [63]. While SnTe is a cubic TCI, it was shown that SnSe is an orthorhombic topological system [64]. Furthermore, it has been shown that SnTe is a helical higher-order topological insulator [65–67]. It has been observed that the characteristic properties change by changing the size or dimensions (1D, 2D or 3D phase) of the materials, namely the properties will change if we move from bulk [27, 68, 69] to thin films [28, 70–74] and to nanowires [75, 76]. For instance, SnTe is a trivial insulator if it has a small thickness, but becomes topological above some critical thickness [77, 78]. In previous works, it was shown that another way

to tune the topological properties is to investigate how the topology changes as a function of composition in $Pb_{1-x}Sn_xTe$ and $Pb_{1-x}Sn_xSe$ [60, 61, 79–81], because in fact PbSe and PbTe are trivial, while SnSe and SnTe are TCI. In the intermediate region between the trivial and TCI phases for rock-salt chalcogenides alloys, the presence of the Weyl phase (WP) has been proposed [82, 83].

In this paper, we will investigate how doping can tune different topological properties such as the trivial insulating phase, topological crystalline phase, and Weyl phase in the quaternary compound of IV–VI semiconductors $Pb_{1-x}Sn_xSe_{1-y}Te_y$. For the first time, we analyze the properties of the quaternary compound $Pb_{1-x}Sn_xSe_{1-y}Te_y$ as a function of the concentrations x and y using the virtual crystal approximation (VCA). We use a density functional theory (DFT) approach and build tight-binding minimal models based on the Wannier transformation of the *ab initio* results. We report different tight-binding models depending on whether we want to reproduce the gap or the Chern number. We are looking at the concentration that leads to the transition from a topologically trivial phase to a non-trivial phase. With our models, we reproduce the experimental results reasonably well and give an important indication about the transition line from the trivial to topological phase. The Weyl phase predicted in the literature is located in a region of 15% of doping concentration, starting from the point of the closing of the gap in the virtual crystal approximation [82, 83]. The paper is organized as follow: in Sect. 2 we describe the computational details; in Sect. 3 the results are reported with three different Chern number maps obtained with three sets of parameters (Sect. 4); while the last section (Sect. 5) is devoted to conclusions.

2. Computational details

We performed our calculations within the framework of the first-principles density functional theory (DFT) based on the plane-wave basis set and the projector augmented wave method using VASP [84] package. The calculations are fully relativistic by considering the spin–orbit coupling (SOC). A plane-wave energy cut-off of 250 eV was used. We performed the calculations using a $6 \times 6 \times 6$ k-points mesh centered at the Γ point with 216 k-points in the independent Brillouin zone.

For this class of compounds, the generalised gradient approximation (GGA) [85] underestimates the band gap. By using GGA we obtain that the compounds are topological for all concentrations. Several methods have been used in the literature in order to increase the gap, including GGA+U with Coulomb repulsion on the $6s$ orbital of Pb [83]. Instead, we used the meta-GGA approach to the modified Becke–Johnson (MBJ) [86, 87] exchange potential along with GGA for the correlation potential scheme, as already done in previous works for SnTe material class [81, 88] and other narrow gap semiconductors [89, 90]. We used the value of the parameter $c = 1.10$, which gives us good results for the band gap and the mirror Chern number. After obtaining the Bloch's wave functions $\psi_{n,\boldsymbol{k}}$, the p-like anion and cation Wannier functions are build-up using the WANNIER90 code [91]. To determine the real space Hamiltonian in the Wannier function basis, we used the Slater–Koster interpolation scheme and constructed a symmetrized relativistic Wannier tight-binding model using the independent Python package wannhrsymm [92].

We used room temperature lattice constants [93] reduced by 0.5% in order to consider the temperature effect. The lattice constant used for the zero kelvin DFT calculations are $a_{\mathrm{SnTe}} = 6.2964$ Å, $a_{\mathrm{PbTe}} = 6.4277$ Å, and $a_{\mathrm{PbSe}} = 6.0954$ Å.

3. Mirror Chern number calculation

We used the virtual crystal approximation (VCA) to estimate the transition between topologically trivial and non-trivial phases. We analysed the trend of the mirror Chern number (MCN) for the quaternary compound $Pb_{1-x}Sn_xSe_{1-y}Te_y$ as a function of the concentrations x and y. Next, we studied the transition from the trivial to the topological phase as a function of x and y. The VCA Hamiltonian that describes the alloy is

$$H(x,y) = xH_{\mathrm{SnTe}} + (y-x)H_{\mathrm{PbTe}} + (1-y)H_{\mathrm{PbSe}}, \tag{1}$$

where H_{PbTe}, H_{PbSe}, and H_{SnTe} are symmetrized, relativistic Wannier tight-binding Hamiltonians for the PbTe, PbSe, and SnTe compounds, respectively. We have excluded SnSe from (1) because it has a different structure, i.e., rhombohedral instead of cubic, and it is far from transition. Note that the Hamiltonian (1) exhibits mirror symmetries and time-reversal symmetries.

The mirror operator with respect to the $(\bar{1}10)$ plane is

$$M_{xy} = \frac{(\sigma_x - \sigma_y)}{\sqrt{2}} \otimes \Big(\mathbb{I}_3 - L_z^2 - \big[L_x, L_y\big]\Big) \otimes P_{xy}. \tag{2}$$

It is a Kronecker product of three parts related to the spin, the orbital and the atomic degrees of freedom. In (2), σ_x and σ_y are the Pauli matrices, $\mathbb{I}_n$ is the $n \times n$ identity matrix, L_i with $i = x, y, z$ are the orbital angular momentum operators for $l = 1$, and P_{xy} is the matrix that exchanges the atomic positions with respect to the mirror plane, the form of which depends on our choice of vector basis.

The time-reversal operator is $T = \sigma_y \otimes \mathbb{I}_3 \otimes \mathbb{I}_8$ and it is also a product of three parts; the first related to the spin, the second to the orbital, and the third to the atoms.

These operators $M_{x,y}$ and T verify the following relations

$$M_{xy} H\big(k_x, k_y, k_z\big) M_{xy}^{\dagger} = H\big(k_y, k_x, k_z b\big), \tag{3}$$

$$T H\big(k_x, k_y, k_z\big) T^{\dagger} = H\big(-k_x, -k_y, -k_z\big), \tag{4}$$

and the mirror operator anticommutes with the time-reversal operator. In the eigenbasis of the mirror operator, the time-reversal operator takes the off-diagonal block form, and the Hamiltonian commutes with the mirror operator. Therefore, it has a block-diagonal form. This leads MCNs to vanish on high symmetry planes, where each block has the opposite MCN. To calculate MCN, which we define as C from now on, we use the Kubo formula

$$C = \frac{1}{\pi}\int_0^{2\pi}\int_0^{2\pi} \mathrm{d}k_x\,\mathrm{d}k_z \sum_{n\le n_F, n'>n_F} \mathrm{Im}\left(\frac{\langle n|\partial_{k_x}H|n'\rangle\langle n'|\partial_{k_z}H|n\rangle}{(\epsilon_n-\epsilon_{n'})^2}\right), \tag{5}$$

where $|n\rangle$ and ϵ_n are the eigenstates and the eigenvalues of the Hamiltonian in the projected subspace, and n_F is the filling. When $C=0$ we have a trivial insulator, while when $C=2$ we have TCI.

4. Realistic and transferable tight-binding model for PbSe, PbTe and SnTe

Here, we report the minimal tight-binding models for selected compounds that reasonably well reproduce the properties of the quaternary compound $Pb_{1-x}Sn_xSe_{1-y}Te_y$ as a function of the concentrations x and y. It is not possible to fit both the gap and the closure of the trivial band gap with a simplified tight-binding Hamiltonian. Therefore, each model presented here focuses on one property that we want to reproduce. We report (i) a model reproducing the experimental band gaps at the L point and at $T=0$ for PbTe and PbSe and the theoretical band gap for SnTe (Table I), (ii) a Hamiltonian fitting the closure of the trivial band gap (Table II), and (iii) a model reproducing experimental band gaps at $T=0$ for PbTe, PbSe, and SnTe (Table III).

In Tables I–III, we show the on-site energies ϵ, the first and the second neighbour hopping parameters, and the spin–orbit coupling λ constants of our tight-binding models for SnTe, PbTe, and PbSe [81]. The first neighbour hopping is the cation–anion hopping; the second ones are anion–anion (aa) and cation–cation (cc) hopping terms. By $t^{lmn}_{\alpha,\beta}$ we denote the hopping amplitudes along the connecting direction $l\boldsymbol{x}+m\boldsymbol{y}+n\boldsymbol{z}$ between the orbitals α and β. We also indicate the chemical bonds σ and π.

We used the DFT values as reported in [81] for all parameters except $V^{110}_{\sigma\mathrm{cc}}$. For $V^{110}_{\sigma\mathrm{cc}}$, we vary its value depending on whether we want to reproduce the experimental band gap [94] or the Chern number. We used the same procedure for PbSe, PbTe, and SnTe. The decision to modify $V^{110}_{\sigma\mathrm{cc}}$ is due to the fact that all hoppings beyond the second nearest neighbours have been cut, and the larger parameters we cut concern the cation–cation hybridization, so in this way, we balanced the contribution due to cations and anions.

In the next three subsections, we report three tight-binding minimal models and the associated Chern number map for different cases. In the last subsection (Sect. 4.4), we add a Weyl phase to obtain a full topological phase diagram.

TABLE I

Values of electronic parameters of our tight-binding model for SnTe, PbTe, and PbSe. The unit is meV. This Hamiltonian model reproduces the experimental band gap at the L point and at $T=0$ K for PbTe [94] and PbSe [94] and the theoretical band gap for SnTe [25].

		SnTe	PbTe	PbSe
on-site	ϵ_c	1094.6	1855.4	2250.4
	ϵ_a	−1205.4	−646.0	−1206.1
SOC	λ_c	334.5	1068.2	1132.5
	λ_a	524.4	553.8	250.3
cation–anion	V^{100}_{σ}	1916.1	1807.4	1788.9
	V^{100}_{π}	−434.2	−402.6	−353.6
cation–cation	$V^{110}_{\sigma\mathrm{cc}}$	142.9	193.3	465.21
	$V^{110}_{\pi\mathrm{cc}}$	−25.3	−23.8	21.1
anion–anion	$V^{110}_{\sigma\mathrm{aa}}$	−200.8	−90.9	−108.2
	$V^{110}_{\pi\mathrm{aa}}$	248.6	131.5	204.0

TABLE II

Same parameter notation as in Table I, but $V^{110}_{\sigma\mathrm{cc}}$ is modified to $V^{110}_{\sigma\mathrm{cc}}(1+\alpha)$ with $\alpha=0.05$. The unit is meV. This Hamiltonian model reproduces reasonably well the experimental topology, as shown in Fig. 2.

		SnTe	PbTe	PbSe
on-site	ϵ_c	1094.6	1855.4	2250.4
	ϵ_a	−1205.4	−646.0	−1206.1
SOC	λ_c	334.5	1068.2	1132.5
	λ_a	524.4	553.8	250.3
cation–anion	V^{100}_{σ}	1916.1	1807.4	1788.9
	V^{100}_{π}	−434.2	−402.6	−353.6
cation–cation	$V^{110}_{\sigma\mathrm{cc}}$	150.0	202.9	488.5
	$V^{110}_{\pi\mathrm{cc}}$	−25.3	−23.8	21.1
anion–anion	$V^{110}_{\sigma\mathrm{aa}}$	−200.8	−90.9	−108.2
	$V^{110}_{\pi\mathrm{aa}}$	248.6	131.5	204.0

4.1. Tight-binding model to reproduce the experimental band gap of PbSe and PbTe and the theoretical band gap of SnTe

The map obtained with the hoppings reported in Table I is shown in Fig. 1, where the experimental transition points are also indicated. The border separating the trivial and topological regions is not linear, unlike what could be expected from VCA that reproduces the linear Hamiltonian combination. With the values of hopping parameters presented in Table I, we obtain a curve quite close to the experimental points. Further, we reproduce the experimental band gap at the L point and at $T = 0$ K for PbTe [94] and PbSe [94] and the theoretical band gap for SnTe [25], which is -0.185 eV.

4.2. Tight-binding model to reproduce the topology

To improve the agreement with the experimental points in Fig. 1, we act on $V_{\sigma cc}^{110}$ introducing the parameter α, so that the new hybridization will be $V_{\sigma cc}^{110}(1+\alpha)$. In Table II the case with $\alpha = 0.05$ is reported, and in Fig. 2 the map obtained with the Hamiltonian (1) is shown. In this case, we do not reproduce the band gap but we can see in Fig. 2 that the border between the trivial and topological phases is closer to the experimental points. With this choice of the α parameter, we increased the width of the topological region; we verified that if we choose a negative value of the α parameter we go in the other direction, increasing the trivial region of the map. This model well reproduces the closure of the trivial band gap.

TABLE III

Values of the electronic parameters of our tight-binding model for SnTe, PbTe, and PbSe. The unit is meV. Using this Hamiltonian model, we reproduce the experimental band gap at the L point and at $T = 0$ K for PbTe [94] and PbSe [94], and we obtain a good approximation of the experimental band gap for SnTe [94].

		SnTe	PbTe	PbSe
on-site	ϵ_c	1094.6	1855.4	2250.4
	ϵ_a	−1205.4	−646.0	−1206.1
SOC	λ_c	497.3	1068.2	1132.5
	λ_a	581.8	553.8	250.3
cation–anion	V_{σ}^{100}	1916.1	1807.4	1788.9
	V_{π}^{100}	−434.2	−402.6	−353.6
cation–cation	$V_{\sigma cc}^{110}$	213.4	193.3	465.21
	$V_{\pi cc}^{110}$	−25.3	−23.8	21.1
anion–anion	$V_{\sigma aa}^{110}$	−200.8	−90.9	−108.2
	$V_{\pi aa}^{110}$	248.6	131.5	204.0

4.3. Tight-binding model to reproduce the experimental band gaps

Furthermore, in Table III we report the results of the Hamiltonian model that reproduces the experimental band gap of PbSe [94] and PbTe [94] at the L point and at $T = 0$ K, and we obtain a good approximation of the band gap of SnTe [94] at $T = 0$ K. When using this Hamiltonian model, the obtained band gap is 0.145 eV for PbSe, 0.190 eV for PbTe and $\simeq -0.321$ eV for SnTe. In this case, we varied not only $V_{\sigma cc}^{110}$, but also the SOC coupling constants with respect to the other tables. The Chern map obtained with this Hamiltonian model is reported in Fig. 3.

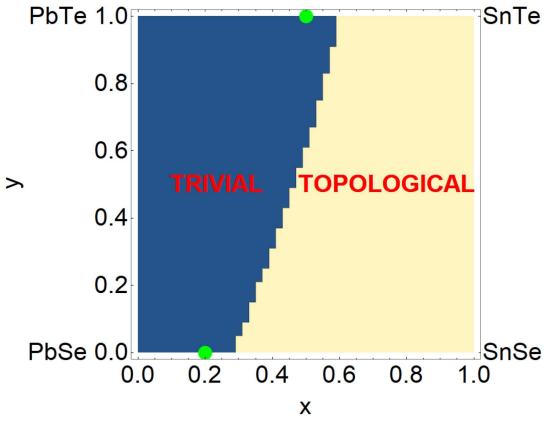

Fig. 1. Mirror Chern number obtained with the Hamiltonian model from Table I for the quaternary compound $Pb_{1-x}Sn_xSe_{1-y}Te_y$ as a function of the concentrations x and y. Using this Hamiltonian, we reproduce the experimental band gap at the L point and at $T = 0$ K for PbTe [94] and PbSe [94] and the theoretical band gap for SnTe [25]. The green circles are the experimental transition points [94]. The blue region represents the trivial phase, while the yellow region represents the topological phase.

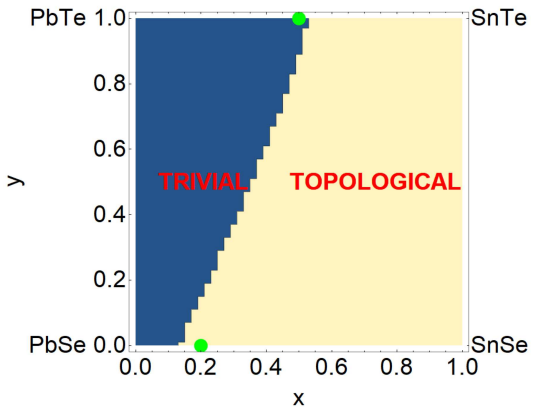

Fig. 2. Description as in Fig. 1, but the results are obtained with the Hamiltonian model from Table II, which reproduces the closure of the trivial gap.

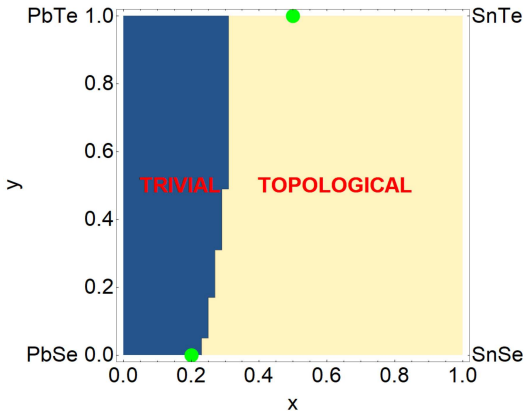

Fig. 3. Description as in Fig. 1, but the results are obtained with the Hamiltonian model from Table III, which reproduces the experimental band gap at the L point and at $T = 0$ K for PbSe, PbTe, and SnTe [94].

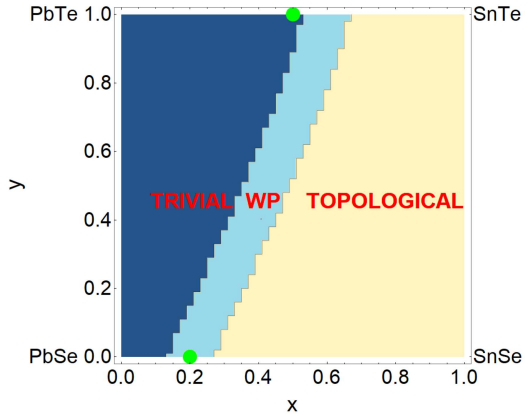

Fig. 4. Complete topological phase diagram obtained using the Hamiltonian model from Table II with the topological phase divided in Weyl semimetallic phase in light blue and topological insulating phase in yellow according to the results reported by Łusakowski et al. [82].

We have tuned the spin-orbit to reproduce the band gap of the pure phases, however, we lose accuracy on the topological transition. Therefore, within this simplified model, we were not able to accurately reproduce both the topological transition and the band gap of the pure phases.

4.4. Weyl phase

Recently, it has been shown that the transition between the topological and trivial phases is broadened [82, 83]. The region where the gap is zero is not a single point, but it is wider — the width is of 15% of the concentration, starting from the point where the gap gets closed. Weyl phase was found in the zero gap region where Wang et al. [83] observe four Weyl points forming two Weyl pairs in the alloy $(PbSe)_{1-x}(SnSe)_x$ by them investigated. They show that the sequential band inversion regime always has a non-zero separation between the Weyl pairs. Therefore, WPs exist not accidentally, but in a wide range within the zero band gap range. This WP is present both if we investigate the alloy under pressure or as a function of concentration.

We also know that VCA is valid close to $x = 0$ and $x = 1$, and that it is less reliable in the intermediate region. The region where VCA does not work well, namely the intermediate region between 0 and 1, coincides with the region of the closure of the band gap where the Weyl phase is present. Since the width of this phase is of 15% of the concentration, starting from the region where the gap gets closed, we can place this phase in the map based on experimental data. In other regions, namely close to 0 and 1, VCA works well, which is why our Chern map is reliable.

In Fig. 4 we report the mirror Chern number map from the parameters given in Table II. The obtained MCN map shows not only the transition line between the trivial insulating phase and the TCI phase, but also the WP region, which is located in an area of 15% of width, starting from the point of the closing of the trivial gap [82, 83].

5. Conclusions

We have built different minimal tight-binding models for the three compounds PbSe, PbTe, and SnTe in order to investigate the topological phase diagram of the quaternary compound $Pb_{1-x}Sn_xSe_{1-y}Te_y$.

We analyzed the properties of the quaternary compound $Pb_{1-x}Sn_xSe_{1-y}Te_y$ for the first time, because previously only ternary compounds $Pb_{1-x}Sn_xTe$ and $Pb_{1-x}Sn_xSe$ have been studied. The transition between the trivial phase and the topological phase, driven by the x content of Sn, was investigated in previous works, but a full phase map for these compounds had not yet been provided. We built up a model that can reproduce the entire Chern map for a quaternary compound, and we give the experimentalists indications of the border between the trivial and the topological phases. The experimental transition line between the trivial and topological phases is not available because only ternary compounds were studied, however with one of our sets of hopping parameters we obtain a good agreement with the experimental points related to the ternary compounds $Pb_{1-x}Sn_xTe$ and $Pb_{1-x}Sn_xSe$. Another important information we get is that the border between the trivial and topological regions is not linear to what can be expected if the virtual crystalline approximation is used.

Furthermore, since we know from previous studies that the region where the gap is closed is not a single point but wider, and the width is of the 15% of the concentration starting from the point where the gap gets closed, we give an indication of the position of this region in the Chern map.

After obtaining the tight-binding parameters extracted from *ab initio*, we tuned the parameter $V_{\sigma cc}^{110}$ to improve the agreement with the transition of the mirror Chern number at $y = 0$ and $y = 1$ observed in experimental results. Eventually, we satisfactory reproduce the topological transition line close to the experimental transition points at $y = 0$ and $y = 1$, and we also add the location of the Weyl phase predicted in the literature [83], producing the full topological phase diagram for the $Pb_{1-x}Sn_xSe_{1-y}Te_y$ quaternary compound.

Acknowledgments

We thank V. Volobuiev, R. Buczko, and T. Hyart for useful discussions. The work is supported by the Foundation for Polish Science through the International Research Agendas program co-financed by the European Union within the Smart Growth Operational Programme. We acknowledge the access to the computing facilities of the Interdisciplinary Center of Modeling at the University of Warsaw, Grant G84-0, GB84-1, and GB84-7. We acknowledge the CINECA award under the ISCRA initiative IsC85 "TOPMOST" and IsC93 "RATIO" grant, for the availability of high-performance computing resources and support.

References

[1] T. Dietl, A. Bonanni, H. Ohno, *J. Semicond.* **40**, 080301 (2019).

[2] T. Dietl, K. Sato, T. Fukushima, A. Bonanni, M. Jamet, A. Barski, S. Kuroda, M. Tanaka, P.N. Hai, H. Katayama-Yoshida, *Rev. Mod. Phys.* **87**, 1311 (2015).

[3] T. Dietl, *Acta Phys. Pol. A* **139**, 355 (2021).

[4] H. Kepa, V.K. Le, C.M. Brown, M. Sawicki, J.K. Furdyna, T.M. Giebultowicz, T. Dietl, *Phys. Rev. Lett.* **91**, 087205 (2003).

[5] S. Hümpfner, K. Pappert, J. Wenisch, K. Brunner, C. Gould, G. Schmidt, L.W. Molenkamp, M. Sawicki, T. Dietl, *Appl. Phys. Lett.* **90**, 102102 (2007).

[6] J. Ruan, S.-K. Jian, H. Yao, H. Zhang, S.-C. Zhang, D. Xing, *Nat. Commun.* **7**, 1 (2016).

[7] C. Sliwa, C. Autieri, J.A. Majewski, T. Dietl, *Phys. Rev. B* **104**, L220404 (2021).

[8] Y. Qian, J. Gao, Z. Song, S. Nie, Z. Wang, H. Weng, Z. Fang, *Phys. Rev. B* **101**, 155143 (2020).

[9] R. Islam, B. Ghosh, G. Cuono, A. Lau, W. Brzezicki, A. Bansil, A. Agarwal, B. Singh, T. Dietl, C. Autieri, *Phys. Rev. Res.* **4**, 023114 (2022).

[10] D.J. Campbell, J. Collini, J. Slawińska et al., *npj Quantum Mater.* **6**, 38 (2021).

[11] A.S. Wadge, B.J. Kowalski, C. Autieri, P. Iwanowski, A. Hruban, N. Olszowska, M. Rosmus, J. Kołodziej, A. Wiśniewski, *Phys. Rev. B* **105**, 235304 (2022).

[12] M. König, S. Wiedmann, C. Brüne, A. Roth, H. Buhmann, L.W. Molenkamp, X.-L. Qi, S.-C. Zhang, *Science* **318**, 766 (2007).

[13] Z. Zhu, G.W. Winkler, Q. Wu, J. Li, A.A. Soluyanov, *Phys. Rev. X* **6**, 031003 (2016).

[14] W. Lei, W. Wang, X. Ming, S. Zhang, G. Tang, X. Zheng, H. Li, C. Autieri, *Phys. Rev. B* **101**, 205149 (2020).

[15] N. Pournaghavi, M.F. Islam, R. Islam, C. Autieri, T. Dietl, C.M. Canali, *Sci. Rep.* **103**, 195308 (2021).

[16] R. Islam, S. Mardanya, A. Lau, G. Cuono, T.-R. Chang, C.M. Canali, B. Singh, T. Dietl, C. Autieri, "Engineering an Axion Insulator Phase in Superlattices without Inversion Symmetry", submitted (2022).

[17] A. Lau, T. Hyart, C. Autieri, A. Chen, D.I. Pikulin, *Phys. Rev. X* **11**, 031017 (2021).

[18] T.C. van Thiel, J. Fowlie, C. Autieri, N. Manca, M. Siškins, D. Afanasiev, S. Gariglio, A.D. Čaviglia, *ACS Mater. Lett.* **2**, 389 (2020).

[19] T.C. van Thiel, W. Brzezicki, C. Autieri et al., *Phys. Rev. Lett.* **127**, 127202 (2021).

[20] C. Autieri, P.A. Kumar, D. Walecki, S. Webers, M.A. Gubbins, H. Wende, B. Sanyal, *Sci. Rep.* **1**, 29307 (2016).

[21] C. Autieri, B. Sanyal, *New J. Phys.* **16**, 113031 (2014).

[22] A. Paul, C. Reitinger, C. Autieri, B. Sanyal, W. Kreuzpaintner, J. Jutimoosik, R. Yimnirun, F. Bern, P. Esquinazi, P. Korelis, P. Böni, *Appl. Phys.* **105**, 022409 (2014).

[23] C. Autieri, M. Cuoco, C. Noce, *Phys. Rev. B* **85**, 075126 (2012).

[24] R. Basnet, K.M. Kotur, M. Rybak, C. Stephenson, S. Bishop, C. Autieri, M. Birowska, J. Hu, *Phys. Rev. Res.* **4**, 023256 (2022).

[25] T.H. Hsieh, H. Lin, J. Liu, W. Duan, A. Bansil, L. Fu, *Nat. Commun.* **3**, 1 (2012).

[26] P. Barone, D. Di Sante, S. Picozzi, *Phys. Status Solidi Rapid Res. Lett.* **7**, 1102 (2013).

[27] P. Barone, T.C.V. Rauch, D. Di Sante, J. Henk, I. Mertig, S. Picozzi, *Phys. Rev. B* **88**, 045207 (2013).

[28] V.V. Volobuev, P.S. Mandal, M. Galicka et al., *Adv. Mater.* **29**, 1604185 (2017).

[29] L. Fu, C.L. Kane, E.J. Mele, *Phys. Rev. Lett.* **98**, 106803 (2007).

[30] S. Sun, Z. Song, H. Weng, X. Dai, *Phys. Rev. B* **101**, 125118 (2020).

[31] A.S. Wadge, G. Grabecki, C. Autieri et al., *J. Phys. Condensed Matter* **34**, 125601 (2022).

[32] Y. Chen, Y.-M. Lu, H.-Y. Kae, *Nat. Commun.* **6**, 6593 (2015).

[33] N. Manca, D.J. Groenendijk, I. Pallecchi, C. Autieri, L.M.K. Tang, F. Telesio, G. Mattoni, A. McCollam, S. Picozzi, A.D. Caviglia, *Phys. Rev. B* **97**, 081105 (2018).

[34] A. Daido, T. Yoshida, Y. Yanase, *Phys. Rev. Lett.* **122**, 227001 (2019).

[35] C. Autieri, C. Noce, *Philos. Mag.* **97**, 3276 (2017).

[36] C. Autieri, G. Cuono, F. Forte, C. Noce, *J. Phys. Condensed Matter* **29**, 224004 (2017).

[37] C. Autieri, G. Cuono, F. Forte, C. Noce, *J. Phys. Conf. Ser.* **969**, 012106 (2018).

[38] G. Cuono, F. Forte, M. Cuoco, R. Islam, J. Luo, C. Noce, C. Autieri, *Phys. Rev. Mater.* **3**, 095004 (2019).

[39] G. Cuono, C. Autieri, G. Guarnaccia, A. Avella, M. Cuoco, F. Forte, C. Noce, *Eur. Phys. J. Special Topics* **228**, 631 (2019).

[40] A. Nigro, G. Cuono, P. Marra, A. Leo, G. Grimaldi, Z. Liu, Z. Mi, W. Wu, G. Liu, C. Autieri, J. Luo, C. Noce, *Materials* **15**, 1027 (2022).

[41] C. Xu, N. Wu, G.-X. Zhi, B.-H. Lei, X. Duan, F. Ning, C. Cao, Q. Chen, *npj Computat. Mater.* **6**, 30 (2020).

[42] G. Cuono, C. Autieri, F. Forte, M.T. Mercaldo, A. Romano, A. Avella, C. Noce, *New J. Phys.* **21**, 063027 (2019).

[43] G. Cuono, F. Forte, A. Romano, X. Ming, J. Luo, C. Autieri, C. Noce, *Phys. Rev. B* **103**, 214406 (2021).

[44] G. Cuono, F. Forte, A. Romano, X. Ming, J. Luo, C. Autieri, C. Noce, *Phys. Rev. Mater.* **5**, 064402 (2021).

[45] T. Dietl, *Acta Phys. Pol. A* **139**, 355 (2021).

[46] H. Wang, Y. Pei, A.D. LaLonde, G.J. Snyder, *Adv. Mater.* **23**, 1366 (2011).

[47] C. Wood, *Rep. Prog. Phys.* **51**, 459 (1988).

[48] A.I. Lebedev, I.A. Sluchinskaya, *Ferroelectrics* **157**, 275 (1994).

[49] P. Liu, H.J. Han, J. Wei, D.J. Hynek, J.L. Hart, M.G. Han, C.J. Trimble, J.R. Williams, Y. Zhu, J.J. Cha, *ACS Appl. Electron. Mater.* **3**, 184 (2021).

[50] Y. Matsushita, P. Wianecki, A.T. Sommer, T. Geballe, I. Fisher, *Phys. Rev. B* **74**, 134512 (2006).

[51] G. Mazur, K. Dybko, A. Szczerbakow, J. Domagala, A. Kazakov, M. Zgirski, E. Lusakowska, S. Kret, J. Korczak, T. Story, M. Sawicki, T. Dietl, *Phys. Rev. B* **100**, 041408(R) (2019).

[52] P. Sessi, D. Di Sante, A. Szczerbakow et al., *Science* **354**, 1269 (2016).

[53] W. Brzezicki, M.M. Wysokiński, T. Hyart, *Phys. Rev. B* **100**, 121107 (2019).

[54] S. Jin, H. Wu, T. Xu, *Appl. Phys. Lett.* **95**, 132105 (2009).

[55] G. Grabecki, *J. Appl. Phys.* **101**, 081722 (2007).

[56] B.A. Akimov, A.V. Dmitriev, D.R. Khokhlov, L.I. Ryabova, *Phys. Status Solidi (a)* **137**, 9 (1993).

[57] Y. Liu, M. Gibbs, J. Puthussery, S. Gaik, R. Ihly, H.W. Hillhouse, M. Law, *Nano Lett.* **10**, 1960 (2010).

[58] L. Fu, *Phys. Rev. Lett.* **106**, 106802 (2011).

[59] A. Lau, C. Ortix, *Phys. Rev. Lett.* **122**, 186801 (2019).

[60] S.-Y. Xu, C. Liu, N. Alidoust et al., *Nat. Commun.* **3**, 1 (2012).

[61] P. Dziawa, B. Kowalski, K. Dybko et al., *Nat. Mater.* **11**, 1023 (2012).

[62] D. Di Sante, P. Barone, E. Plekhanov, S. Ciuchi, S. Picozzi, *Sci. Rep.* **5**, 11285 (2015).

[63] A. Lusakowski, P. Bogusławski, T. Story, *Acta Phys. Pol. A* **3**, 141 (2022).

[64] H.J. Zheng, W.J. Shi, C.W. Wang et al., *Phys. Rev. Mater.* **6**, 054201 (2022).

[65] F. Schindler, A.M. Cook, M.G. Vergniory, Z. Wang, S.S. P. Parkin, B.A. Bernevig, T. Neupert, *Sci. Adv.* **4**, eaat0346 (2018).

[66] S.H. Kooi, G. van Miert, C. Ortix, *Phys. Rev. B* **102**, 041122 (2020).

[67] G. van Miert, C. Ortix, *Phys. Rev. B* **98**, 081110 (2018).

[68] E. Plekhanov, P. Barone, D. Di Sante, S. Picozzi, *Phys. Rev. B* **90**, 161108 (2014).

[69] H. Wang, P. Gopal, S. Picozzi, S. Curtarolo, M. Buongiorno Nardelli, J. Sławińska, *npj Computat. Mater.* **6**, 7 (2020).

[70] J. S lawińska, F.T. Cerasoli, P. Gopal, M. Costa, S. Curtarolo, M.B. Nardelli, *2D Materials* **7**, 025026 (2020).

[71] K. Liu, J. Lu, S. Picozzi, L. Bellaiche, H. Xiang, *Phys. Rev. Lett.* **121**, 027601 (2018).

[72] A.V. Galeeva, D.A. Belov, A.S. Kazakov, A.V. Ikonnikov, A.I. Artamkin, L.I. Ryabova, V.V. Volobuev, G. Springholtz, S.N. Danilov, D.R. Khokhlov, *Nanomaterials* **11**, 3207 (2021).

[73] A. Kazakov, W. Brzezicki, T. Hyart et al., *Phys. Rev. B* **103**, 245307 (2021).

[74] R. Rechcinski, M. Galicka, M. Simma et al., *Adv. Funct. Mater.* **31**, 2008885 (2021).

[75] N.M. Nguyen, W. Brzezicki, T. Hyart, *Phys. Rev. B* **105**, 075310 (2022).

[76] G. Hussain, G. Cuono, P. Dziawa , S. Kret, J. Polaczynski, S. Sattar, C.M. Canali, T. Story, J. Sadowski, A. Lau, C. Autieri, "Pentagonal Nanowires from Topological Crystalline Insulators: A Platform for High-Order Topology", submitted (2022).

[77] J. Liu, T.H. Hsieh, P. Wei, W. Duan, J. Moodera, L. Fu, *Nat. Mater.* **13**, 178 (2014).

[78] J. Liu, X. Qian, L. Fu, *Nano Lett.* **15**, 2657 (2015).

[79] Y. Tanaka, Z. Ren, T. Sato, K. Nakayama, S. Souma, T. Takahashi, K. Segawa, Y. Ando, *Nat. Phys.* **8**, 800 (2012).

[80] B.M. Wojek, P. Dziawa, B. Kowalski, A. Szczerbakow, A.M. Black-Schaffer, M. Berntsen, T. Balasubramanian, T. Story, O. Tjernberg, *Phys. Rev. B* **90**, 161202 (2014).

[81] R. Islam, G. Cuono, M.N. Nguyen, C. Noce, C. Autieri, *Acta Phys. Pol. A* **136**, 667 (2019).

[82] A. Lusakowski, P. Bogusławski, T. Story, *Phys. Rev. B* **98**, 125203 (2018).

[83] Z. Wang, Q. Liu, A. Zunger, *Mater. Horiz.* **6**, 2124 (2019).

[84] G. Kresse, J. Furthmüller, *Phys. Rev. B* **54**, 11169 (1996).

[85] J.P. Perdew, K. Burke, M. Ernzerhof, *Phys. Rev. Lett.* **77**, 3865 (1996).

[86] A. Goyal, P. Gorai, E. Toberer, V. Stevanovic, *NPJ Computat. Mater.* **3**, 42 (2017).

[87] A.D. Beckea, E.R. Johnson, *J. Chem. Phys.* **124**, 194713 (2008).

[88] F. Tran, P. Blaha, *Phys. Rev. Lett.* **102**, 226401 (2009).

[89] C. Autieri, C. Sliwa, R. Islam, G. Cuono, T. Dietl, *Phys. Rev. B* **103**, 115209 (2021).

[90] G. Hussain, G. Cuono, R. Islam, A. Trajnerowicz, J. Jureoczyk, C. Autieri, T. Dietl, *J. Phys. D: Appl. Phys.* (2022).

[91] A.A. Mostofi, J.R. Yates, Y.S. Lee, I. Souza, D. Vanderbilt, N. Marzari, *Comput. Phys. Commun.* **178**, 685 (2008).

[92] D. Gresch, Q. Wu, G.W. Winkler, R. Häuselmann, M. Troyer, A.A. Soluyanov, *Phys. Rev. Mater.* **2**, 103805 (2018).

[93] P.J. McCann, J. Fuchs, Z. Feit, C.G. Fonstad, *J. Appl. Phys.* **62**, 2994 (1987).

[94] R. Dornhaus, G. Nimtz, B. Schlicht, *Narrow gap semiconductors*, Springer Berlin Heidelberg, Berlin 1983.